

The Effect of Volcanic ash Pozzolan and Metakaolin on Electrochemical Corrosion Resistance of 2304 Duplex Stainless Steel Reinforcing in Concrete Subjected to Marine Environment

Wang Yujie*, Zhou Huiwen*, Fu Xu

Department of Architectural Engineering, North China Institute of Aerospace Engineering, Hebei, Langfang, 065000, China

*E-mail: wangyujie88123@163.com

Received: 1 December 2021 / Accepted: 14 January 2022 / Published: 2 February 2022

The corrosion behavior of 2304 duplex stainless steel reinforcing in concrete structures containing natural basaltic volcanic ash pozzolan and metakaolin as partially replacing materials for Portland cement (PC) in 3.5wt% NaCl solution as a marine environment was studied in this work. The corrosion resistance of stainless steel rebars was investigated using polarization assessment, electrochemical impedance spectroscopy (EIS), and a water absorption test. The concrete sample that included both basaltic volcanic ash pozzolan and metakaolin admixtures (BPMK) demonstrated superior steel reinforced concrete corrosion behavior. Water absorption is significantly reduced in the BPMK concrete sample. The passive current density in the BPMK sample was lower than in the other samples, showing that stainless steel reinforced concrete that included both basaltic volcanic ash and metakaolin admixtures has improved corrosion resistance. The EIS results show that the BPMK sample has a significant improvement in polarization resistance value, indicating greater corrosion resistance when compared to other samples.

Keywords: Electrochemical corrosion; Duplex stainless steel reinforcing in concrete; Electrochemical impedance spectroscopy; Polarization test

1. INTRODUCTION

The corrosion resistance of stainless steel in concrete reduces the structure's durability. Corrosion takes place regardless of how well concrete protects steel rebars [1, 2]. Corrosion is caused by corrosive ions penetrating the concrete or the loss of alkalinity [3, 4]. Corrosion control methods include using additives in concrete mortar, corrosion protection, and steel rebar surface coating [5, 6]. The use of additives on their own is appealing due to their low cost. Mineral additives are widely employed in a variety of applications, including high-performance concrete structures, and bridge

structures [7]. Fly ash, silica fume, and blast furnace slag are examples of well-known mineral additions [8, 9]. The use of the components in concrete manufacturing has a beneficial environmental impact and reduces disposal issues [10, 11].

As a result, it has been determined that alternate precursor materials are required. In recent research [12, 13], natural basaltic volcanic ash pozzolan (BVAP) has been presented as a sustainable way of obtaining alkali-activated material. These are widely available in a variety of countries, with little or no use made of them in some situations, generating great interest in their application as a precursor to alkali-activated materials [14-16]. The amount of research using BVAP-based alkali-activated materials has continuously increased, focusing mostly on mechanical and physical qualities, with few findings on durability features [17-19]. However, no evaluation studies on the corrosion-performance of stainless steel in BVAP-based concrete in chloride-ion-rich settings have been reported [20-22]. In general, research on the corrosion-performance of reinforcing steel is restricted, with most studies focused on the performance of BVAP/metakaolin-based concrete. In this study, the electrochemical corrosion behaviors of 2304 duplex stainless steel reinforced in concrete with BVAP and metakaolin were investigated. The corrosion resistance of stainless steel rebar was investigated using polarization evaluation, electrochemical impedance spectroscopy (EIS) assessment, and open-circuit potential (OCP) characterization.

2. MATERIALS AND METHOD:

Electrochemical and compressive strength assessments were done on specimens to study the electrochemical and mechanical properties of concrete specimens replaced with basaltic volcanic ash pozzolan (BVAP) and metakaolin. The various components of cement for the construction of reinforced concrete were used in this study, which included varying mixing percentages of Portland cement (PC), BVAP, and metakaolin. The chemical characteristics of cement admixtures are shown in Table 1.

Table 1. Chemical properties of PC, BVAP and metakaolin

| | PC (wt%) | BVAP(wt%) | Metakaolin (wt%) |
|------------------------------------|----------|-----------|------------------|
| SiO₂ | 21.42 | 46.41 | 52.16 |
| Al₂O₃ | 4.73 | 14.39 | 40.83 |
| MgO | 2.14 | 8.26 | 0.16 |
| Fe₂O₃ | 3.18 | 12.69 | 0.95 |
| CaO | 63.21 | 8.12 | 0.22 |
| K₂O | 0.72 | 1.97 | 0.17 |
| Na₂O | 0.24 | 3.35 | 0.01 |
| SO₃ | 2.88 | 0.00 | 0.00 |
| LOI | 0.85 | 1.34 | 0.58 |

Table 2 displays the mix proportions for each sample. To make concrete, the PC was mixed with gravel, sand, and water (1.5: 1: 3: 0.5). Prepared mixes were poured into cylindrical molds that had a radius of 8cm and a height of 20cm. After that, the samples were maintained at a temperature of 24°C for one day.

Table 2. Mix proportions for various concrete structures

| Mixtures | PC(wt%) | BVAP(wt%) | Metakaolin(wt%) |
|-------------|---------|-----------|-----------------|
| PC | 100.0 | 0.0 | 0.0 |
| MK | 70.0 | 0.0 | 30.0 |
| BP | 70.0 | 30.0 | 0.0 |
| BPMK | 70 | 15 | 15 |

Electrochemical tests were conducted to consider the effects of BVAP and metakaolin admixtures on the corrosion resistance of 2304 duplex stainless steel rebar. In the cylindrical mold, the concrete mix was then poured to make the working electrode, and the stainless steel rebars were put vertically in the middle of the cylinder. The stainless steel rebar had a diameter of 1cm and a length of 15cm. Table 3 shows the chemical composition of the steel that was used.

Table 3. Composition of 2304 DS steel rebar (wt%)

| Carbon(C) | Silicon(Si) | Sulfur(S) | Chromium(Cr) | Manganese(Mn) | Phosphorus(P) | Nickel(Ni) | Iron(Fe) |
|-----------|-------------|-----------|--------------|---------------|---------------|------------|----------|
| 0.02 | 0.85 | 0.01 | 23.01 | 1.8 | 0.03 | 4.00 | Residual |

According to ASTM C109-16a, the compressive strength was measured. The following equation will be used to calculate compressive strength [23]:

$$S(\text{N/mm}^2) = \text{Ultimate load(N)} / \text{Sample area(mm}^2\text{)} \quad (1)$$

A high-impedance voltmeter with a $10\text{M}\Omega$ input resistance was used to measure the open circuit potential (OCP) for the various systems on a regular basis. In order to simulate a marine environment, all reinforced concrete was subjected to a 3.5wt% NaCl media. Using specialist software, the acquired results were analyzed. A three-electrode electrochemical system, including of the stainless steel rebar, graphite and a standard copper/copper sulfate electrode were used as the working, counter and reference electrodes, respectively. The EIS measurements were performed using a 10mV AC perturbation in the frequency range of 100 kHz to 0.1mHz. The polarization experiment was carried out at a 1mV/s scanning rate. ASTM C642 was used to assess water absorption. The surface morphologies of the specimens were studied by the Zeiss Sigma 300 VP scanning electron microscope (SEM).

3. RESULTS AND DISCUSSION

Fig. 1 shows the compressive strength values of various specimens after 4-weeks of immersion. As shown in Fig. 1, the BPMK mixture exhibited a higher compressive strength compared to other samples, which was 5.6 times higher than PC samples. The use of basaltic volcanic ash as a filler in modifying concrete construction may be responsible for the increase in compressive strength in BPMK samples. In addition, the basaltic volcanic ash acts as a pozzolanic reaction activator, forming denser and smaller structures that speed up the hydration process and increase compressive strength [24, 25].

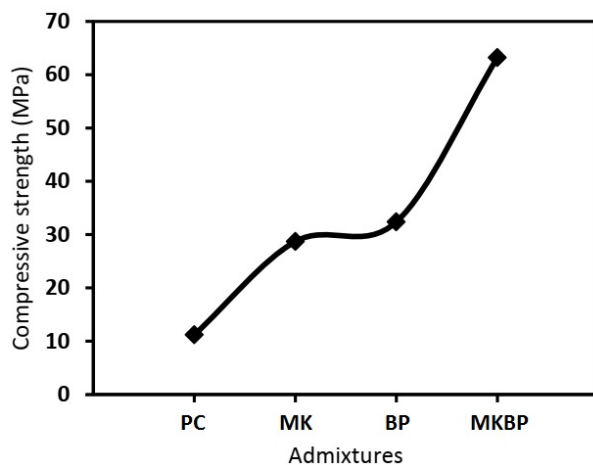


Figure 1. Compressive strength of different concrete specimens after 4-weeks immersion time at room temperature

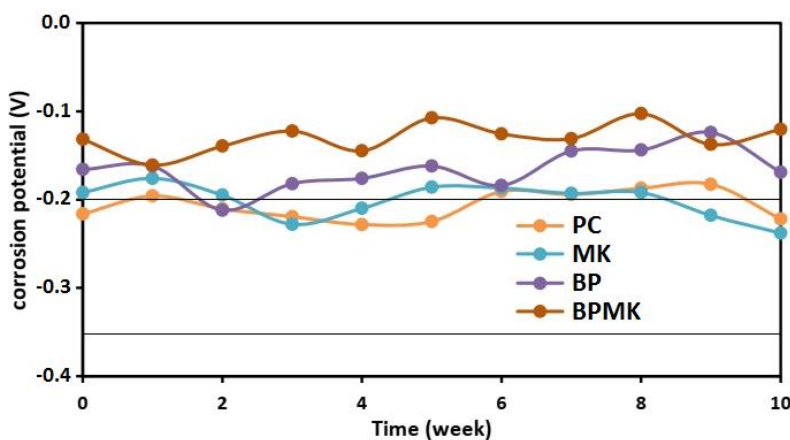


Figure 2. The open circuit potential of samples subjected to a 3.5wt% NaCl solution at different immersion time

Figure 2 shows the open circuit potential of samples subjected to a 3.5wt% NaCl solution, indicating that samples containing basaltic volcanic ash have a 10% corrosion probability for the entire immersion time, with a corrosion potential greater than -200 mV. The samples without basaltic volcanic ash revealed showed an uncertain corrosion for several weeks with a potential value between

-300mV and -200mV, which was linked to the onset of pitting corrosion or a slight separation of the passive film [26, 27].

The open circuit potential results for the BPMK sample were more stable than the other samples' potential values, which remained totally within the 10% corrosion probability band. Because of the reduction in $\text{Ca}(\text{OH})_2$, solubility of hydration products, and changes in pore solution, one of most important aspects of basaltic volcanic ash is its major influence on concrete durability [28].

Figure 3 displays polarization plots of stainless steel reinforced concrete in various admixtures after six months of exposure to a 3.5wt% NaCl solution. Anodic polarization plots at all stainless steel rebars are analyzed by passive areas, as shown in Fig. 2, suggesting that passive films have formed on the surface of the steel once the steel rebars were subjected to the marine environment [29, 30]. Besides, a significant shift in corrosion potential in a positive direction was detected, demonstrating that changing admixtures in concrete structures effectively slowed anodic metal dissolution.

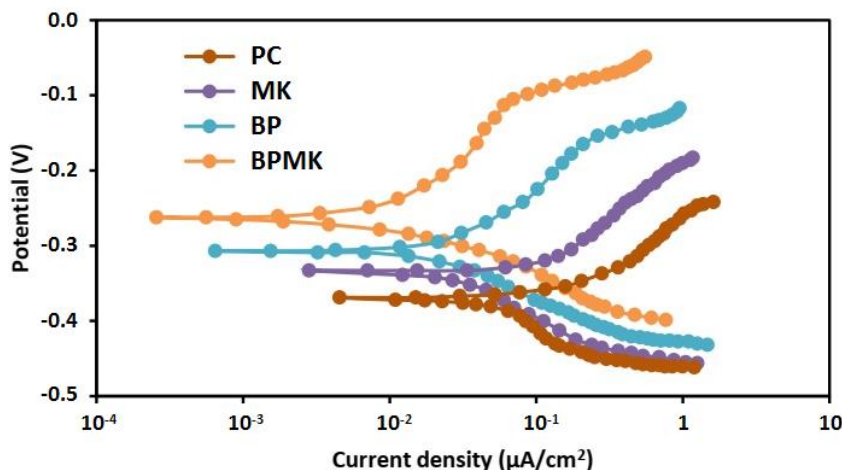


Figure 3. The polarization of stainless steel reinforced concrete containing different mixes exposed to 3.5wt% NaCl media after 4 months at scan rate of 1mV/s

Table 4. Obtained corrosion parameters from polarization plots

| Mixes | Corrosion current density($\mu\text{A}/\text{cm}^2$) | Corrosion potential(V) | $\beta_c(\text{mVdec}^{-1})$ | $-\beta_a(\text{mVdec}^{-1})$ |
|-------------|--|------------------------|------------------------------|-------------------------------|
| PC | 0.32 | -0.353 | 39 | 18 |
| MK | 0.07 | -0.322 | 42 | 23 |
| BP | 0.05 | -0.304 | 44 | 27 |
| BPMK | 0.02 | -0.269 | 38 | 32 |

The BPMK sample had a substantially larger passive zone than the other samples. Furthermore, the BPMK sample had a lower passive current density than the other samples, showing that stainless steel reinforced concrete having both basaltic volcanic ash and metakaolin admixtures has better corrosion resistance. Because basaltic volcanic ash reacted with free $\text{Ca}(\text{OH})_2$ during the cement

hydration process, forming more calcium silicate hydrate, the concrete structures' strength and durability improved [31, 32]. Table 4 shows the corrosion parameters derived from the polarization plots in Fig. 3.

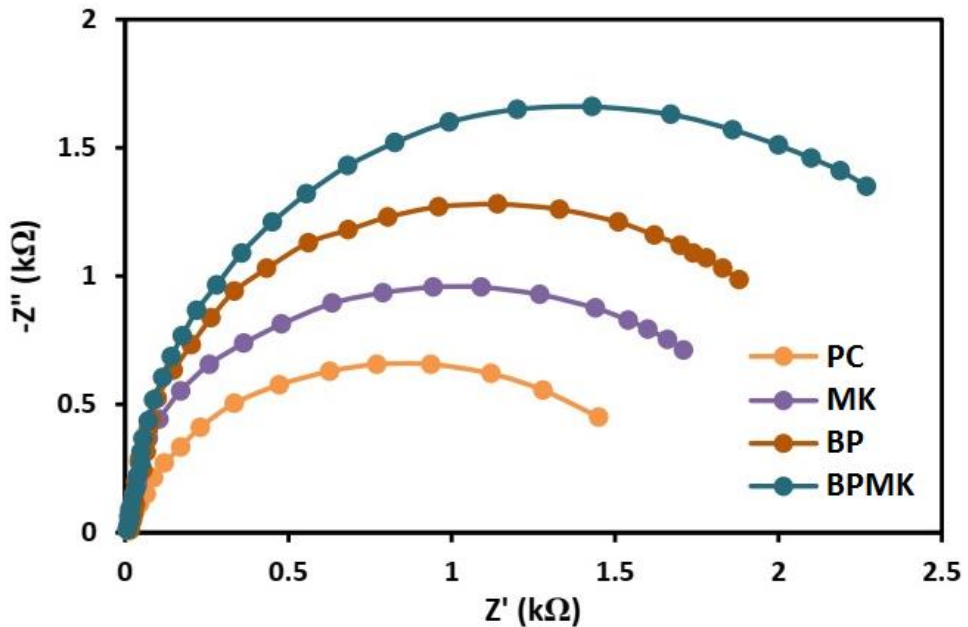


Figure 4. Nyquist plots of stainless steel reinforced concrete containing different mixes subjected to 3.5wt% NaCl media after 4 months at the frequency range of 100 kHz to 0.1mHz.

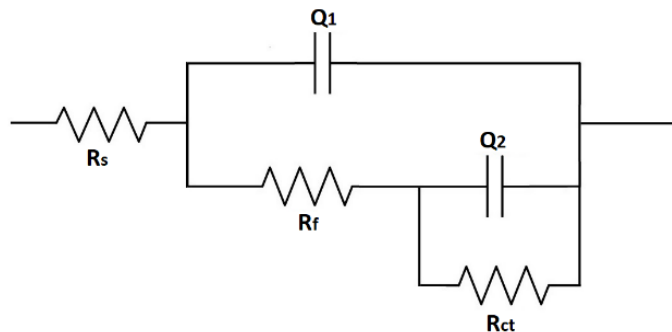


Figure 5. An equivalent circuit model

Because of its ability to characterize redox reactions of stainless steel in a marine environment, the EIS technique has been extensively used in the analysis of passive layers of rebars [33, 34]. EIS was used to investigate the effect of basaltic volcanic ash and metakaolin on the corrosive behavior of stainless steel rebars with passive layers in 3.5% NaCl solution. Figure 4 shows that increasing the amount of basaltic volcanic ash increase the capacitive loop radius, indicating a rise in the corrosion resistance of the reinforced concrete. It is because of the creation of a passive layer [35, 36]. Figure 5 depicts an equivalent circuit for modeling impedance spectra. R_s denotes the solution's resistance. R_f

and R_{ct} are passive layer resistance and charge-transfer resistance, respectively. The passive layer/solution interface capacitance and double-layer capacitance are represented by Q_1 and Q_2 , respectively [37, 38].

Table 5. Electrochemical parameters obtained from the fitting equivalent circuit model

| Mixes | $R_s(\Omega \text{ cm}^2)$ | $R_f(\text{k}\Omega \text{ cm}^2)$ | $Q_1(\mu\text{F cm}^{-2})$ | $R_{ct}(\text{k}\Omega \text{ cm}^2)$ | $Q_2(\mu\text{F cm}^{-2})$ |
|-------------|----------------------------|------------------------------------|----------------------------|---------------------------------------|----------------------------|
| PC | 22.4 | 0.86 | 3.9 | 1.86 | 6.4 |
| MK | 28.6 | 1.13 | 1.2 | 2.35 | 4.3 |
| BP | 31.5 | 1.62 | 1.8 | 2.65 | 5.5 |
| BPMK | 26.7 | 2.97 | 7.6 | 3.36 | 8.2 |

As seen in table 5, the value of Q_2 reduces with the use of basaltic volcanic ash, indicating that passive layer thickness has been enhanced and the resultant protective capacity has been enhanced when the basaltic volcanic ash and metakaolin admixture were simultaneously used in the concrete structure. The R_f passive film resistance will increase as the basaltic volcanic ash content in the alloy increases, indicating that the protective characteristics of the advanced passive layer are strong. When Q_1 and Q_2 are compared, Q_1 is found to be lower than Q_2 , confirming the creation of a passive thin layer and the double layer's high capacitive behavior at the interfaces [39]. Furthermore, the BPMK sample was more resistant to the passive layer compared to the other samples, indicating that the corrosion resistance of the stainless steel rebar surface has increased further.

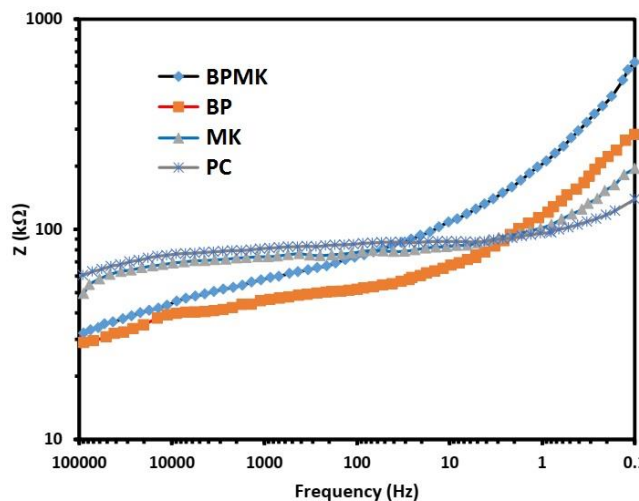


Figure 6. Bode plots of stainless steel reinforced concrete containing different mixes subjected to 3.5wt% NaCl media after 4 months.

The Bode diagrams attained from the EIS results are revealed in Fig. 6. Figure 6 shows that BPMK sample, and then BP sample indicate the best performance to inhibit the corrosion behavior in the steel reinforced concrete. These results are significantly consistent with the EIS measurement findings.

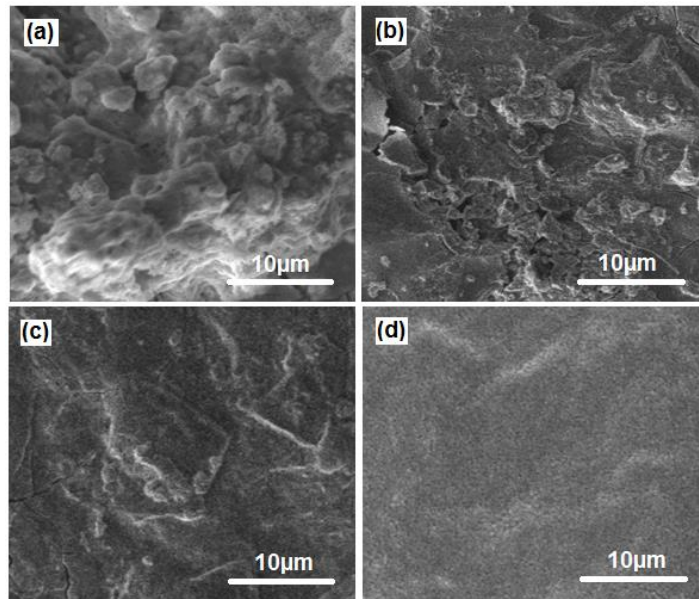


Figure 7. FESEM images of stainless steel rebars in various concrete specimens (a) PC (b) MK (c) BP and (d) BPMK after 4-month subjected to 3.5wt% NaCl solution at room temperature.

Figure 7 depicts the surface morphology of steel rebars in various concrete specimens after four months in the marine environment. The surface of the BPMK specimen reveals poor corrosion products and tiny pits, implying small pitting corrosion formed onto the surface of steel reinforcement bars, which is in line with the electrochemical measurements. It can be related to chloride ion reduction and water permeability in reinforced concrete specimens. The addition of basaltic volcanic ash to the cement paste can change the structure of the large pores into smaller pores. Because of the decrease in Cl^- ions and water permeability, basaltic volcanic ash admixtures in PC resulted in a reduction in corrosion rate and improved corrosion protection of stainless steel rebar.

Figure 8 depicts the water absorption of concrete specimens with various admixtures after one week, one month, two months, and four months immersed in a 3.5% NaCl solution. As seen in Fig. 8, when the exposure time was increased, all of the admixture samples showed a decrease in water absorption compared to the PC samples. This implies that basaltic volcanic ash and metakaolin admixtures in PC could really decrease the concrete structure's water absorption after being immersed in a salty environment [40, 41]. As a result, when both admixtures are used, the samples' water absorption decreases. Even though the existence of water is needed in the early phases of corrosion, adsorption and permeability of samples do not play a significant role in the corrosion behavior of stainless steel rebars, which is in relation to previous research.

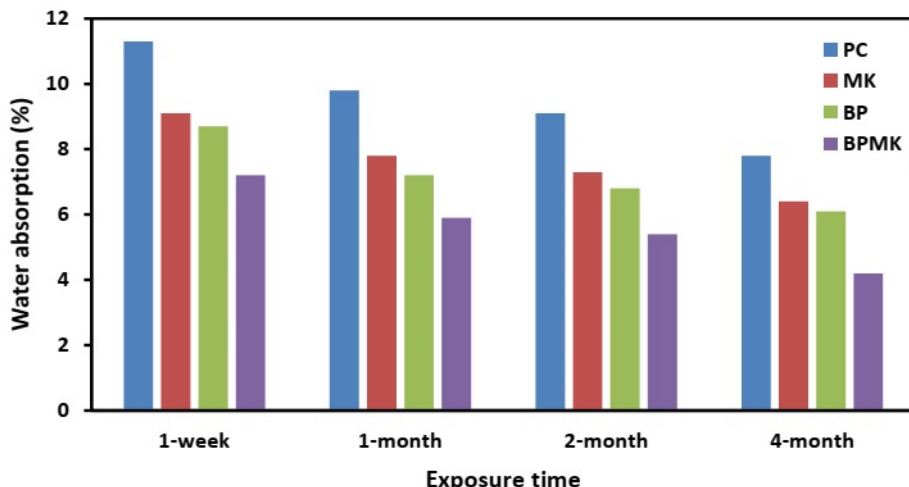


Figure 8. Water absorption of concrete structures with various admixtures at 3.5% NaCl solution after different immersion times

4. CONCLUSIONS

The effects of metakaolin and basaltic volcanic ash admixtures on the concrete compressive strength and corrosion resistance of 2304 DS steel rebars were investigated in this study. The stainless steel reinforced concrete samples were immersed in a 3.5wt% NaCl media. The mechanical findings for concrete samples revealed that the BPMK had a significant effect on the compressive strength. The EIS results showed that the Q2 value decreased for specimens having both basaltic volcanic ash and metakaolin, indicating that the passive film thickness had risen, leading to increased protective capacity. According to the electrochemical results, the BPMK sample had a higher corrosion resistance value compared to the other specimens. The surface morphology of stainless steel rebars revealed narrow pits and low corrosion production on the BPMK sample, which was consistent with the electrochemical test results.

ACKNOWLEDGEMENT

This study was supported by Hebei province institutions of higher learning science and technology research project fund “Correlation and Variability Analysis of geotechnical parameters and zonal study of engineering geology in soft soil foundation of Hebei Province”(QN2017003) and Hebei province construction science and technology research guidance project fund “Research on anchoring mechanism and Optimal design method of anti-floating reaming bolt in underground structure”(20182051).

References

1. S. Jain and B. Pradhan, *Advances in Civil Engineering Materials*, 9 (2020) 463.
2. S. Kakooei, H.M. Akil, M. Jamshidi and J. Rouhi, *Construction and Building Materials*, 27 (2012) 73.

3. P. Woyciechowski, P. Łukowski, E. Szmigiera, G. Adamczewski, K. Chilmon and S. Spodzieja, *Construction and Building Materials*, 303 (2021) 124388.
4. L. Sun, C. Li, C. Zhang, Z. Su and C. Chen, *International Journal of Structural Stability and Dynamics*, 18 (2018) 1840001.
5. M.P. Kumar, K. Mini and M. Rangarajan, *Construction and Building Materials*, 182 (2018) 249.
6. J. Xu, Z. Wu, H. Chen, L. Shao, X. Zhou and S. Wang, *Arabian Journal for Science and Engineering*, 46 (2021) 11319.
7. S. Kakooei, H.M. Akil, A. Dolati and J. Rouhi, *Construction and Building Materials*, 35 (2012) 564.
8. M. Ozturk, M. Karaaslan, O. Akgol and U.K. Sevim, *Cement and Concrete Research*, 136 (2020) 106177.
9. Y. Orooji, B. Tanhaei, A. Ayati, S.H. Tabrizi, M. Alizadeh, F.F. Bamoharram, F. Karimi, S. Salmanpour, J. Rouhi and S. Afshar, *Chemosphere*, 281 (2021) 130795.
10. R. Bajpai, K. Choudhary, A. Srivastava, K.S. Sangwan and M. Singh, *Journal of Cleaner Production*, 254 (2020) 120147.
11. Z. Zhang, C. Luo and Z. Zhao, *Natural Hazards*, 104 (2020) 2511.
12. W. Zhang, R. Mazzarello, M. Wuttig and E. Ma, *Nature Reviews Materials*, 4 (2019) 150.
13. A. Kadhim, M. Sadique, R. Al-Mufti and K. Hashim, *Journal of Building Engineering*, 32 (2020) 101766.
14. C. Chen, J. Zuo and Y. Wang, *International Journal of Electrochemical Science*, 15 (2020) 1634.
15. K. Lin and T. Zheng, *International Journal of Electrochemical Science*, 15 (2020) 12329.
16. S. Jiang, Y. Zuo, M. Yang and R. Feng, *Journal of Petroleum Science and Engineering*, 205 (2021) 108809.
17. V.A. Nunes and P.H. Borges, *Construction and Building Materials*, 281 (2021) 122605.
18. Y. Zuo, S. Jiang, S. Wu, W. Xu, J. Zhang, R. Feng, M. Yang, Y. Zhou and M. Santosh, *Basin Research*, 32 (2020) 1328.
19. J. Zhu, Y. Chen, L. Zhang, B. Guo, G. Fan, X. Guan and R. Zhao, *Journal of Cleaner Production*, 295 (2021) 126405.
20. J. Yu, A. Zhang, L. Zhang, Q. Wang, K. Li and H. Wang, *Materials Research Express*, 8 (2021) 095511.
21. H. Huang, M. Huang, W. Zhang and S. Yang, *Structure and infrastructure engineering*, 17 (2021) 1210.
22. H. Maleh, M. Alizadeh, F. Karimi, M. Baghayeri, L. Fu, J. Rouhi, C. Karaman, O. Karaman and R. Boukherroub, *Chemosphere*, (2021) 132928.
23. I. Justo-Reinoso, A. Caicedo-Ramirez, W.V. Srubar III and M.T. Hernandez, *Construction and Building Materials*, 207 (2019) 59.
24. J.N.Y. Djobo, A. Elimbi, H.K. Tchakouté and S. Kumar, *Environmental Science and Pollution Research*, 24 (2017) 4433.
25. W. Liu, Z. Guo, C. Wang and S. Niu, *Construction and Building Materials*, 299 (2021) 124011.
26. M. Talebian, K. Raeissi, M. Atapour, B. Fernández-Pérez, A. Betancor-Abreu, I. Llorente, S. Fajardo, Z. Salarvand, S. Meghdadi and M. Amirnasr, *Corrosion Science*, 160 (2019) 108130.
27. D. Xu, Q. Liu, Y. Qin and B. Chen, *Structural Health Monitoring*, 19 (2020) 1.
28. F. Rajabipour, E. Giannini, C. Dunant, J.H. Ideker and M.D. Thomas, *Cement and Concrete Research*, 76 (2015) 130.
29. J. Shi, D. Wang, J. Ming and W. Sun, *Journal of Materials in Civil Engineering*, 30 (2018) 04018232.
30. Y. Luo, H. Zheng, H. Zhang and Y. Liu, *Advances in Structural Engineering*, (2021) 1.

31. K. Celik, R. Hay, C.W. Hargis and J. Moon, *Construction and Building Materials*, 197 (2019) 803.
32. Y. Li, D.D. Macdonald, J. Yang, J. Qiu and S. Wang, *Corrosion Science*, 163 (2020) 108280.
33. J. Shi, J. Ming, D. Wang and M. Wu, *Corrosion Science*, 174 (2020) 108851.
34. X. Li, Q. Yu, X. Chen and Q. Zhang, *Journal of Magnesium and Alloys*, (2021) 1.
35. X. Gai, Y. Bai, J. Li, S. Li, W. Hou, Y. Hao, X. Zhang, R. Yang and R. Misra, *Corrosion Science*, 145 (2018) 80.
36. M. Rahimi-Golkhandan, S. Danesh and A. Davoodi, *Water Conservation and Management*, 5 (2021) 65.
37. Z. Pilić and I. Martinović, *International Journal of Electrochemical Science*, 12 (2017) 3576.
38. Y. Xie, X. Meng, F. Wang, Y. Jiang, X. Ma, L. Wan and Y. Huang, *Corrosion Science*, 192 (2021) 109800.
39. B. Li, Y. Huan and W. Zhang, *International Journal of Electrochemical Science*, 12 (2017) 10402.
40. G. Cai, T. Noguchi, H. Degée, J. Zhao and R. Kitagaki, *Environmental Science and Pollution Research*, 23 (2016) 7220.
41. A.G. Abetu and A.B. Kebede, *Water Conservation and Management*, 5 (2021) 40.

© 2022 The Authors. Published by ESG (www.electrochemsci.org). This article is an open access article distributed under the terms and conditions of the Creative Commons Attribution license (<http://creativecommons.org/licenses/by/4.0/>).